

Design of Non-Orthogonal Sequences Using a Two-Stage Genetic Algorithm for Grant-Free Massive Connectivity

Nam Yul Yu, *Senior Member, IEEE*

Abstract—In massive machine-type communications (mMTC), grant-free access is a key enabler for a massive number of users to be connected to a base station with low signaling overhead and low latency. In this paper, a two-stage genetic algorithm (GA) is proposed to design a new set of user-specific, non-orthogonal, unimodular sequences for uplink grant-free access. The first-stage GA is to find a subsampling index set for a partial unitary matrix that can be approximated to an equiangular tight frame. Then in the second-stage GA, we try to find a sequence to be masked to each column of the partial unitary matrix, in order to reduce the peak-to-average power ratio of the resulting columns for multicarrier transmission. Finally, the masked columns of the matrix are proposed as new non-orthogonal sequences for uplink grant-free access. Simulation results demonstrate that the non-orthogonal sequences designed by our two-stage GA exhibit excellent performance for compressed sensing based joint activity detection and channel estimation in uplink grant-free access. Compared to algebraic design, this GA-based design can present a set of good non-orthogonal sequences of arbitrary length, which provides more flexibility for uplink grant-free access in mMTC.

Index Terms—Compressed sensing, genetic algorithm, grant-free access, machine-type communications, non-orthogonal multiple access, peak-to-average power ratio.

I. INTRODUCTION

MASSIVE connectivity of wireless devices is essential for industrial, commercial, and critical applications of massive machine-type communications (mMTC) [1], [2], which provides a concrete platform for the Internet of Things (IoT). Unlike human-type communications (HTC), mMTC is characterized by small size data, infrequent transmission, low cost devices, low mobility, and so on [3]. In practice, mMTC systems need to support a massive number of devices with low control overhead, low latency, and low power consumption for delay-sensitive and energy efficient communications.

Non-orthogonal multiple access (NOMA) [4], [5] has received a great deal of attention for massive connectivity in 5G wireless systems. In code-domain NOMA, user-specific and non-orthogonal spreading sequences are assigned to users for their non-orthogonal multiplexing through common resources. In sparse code multiple access (SCMA) [6], sparse spreading sequences are assigned to users, where a message passing

algorithm (MPA) [7] and a list sphere decoding based MPA decoder [8] can be deployed for reliable multiuser detection with low complexity. Complex-valued spreading sequences are employed for multi-user shared access (MUSA) [9], where the successive interference cancellation (SIC) can be performed for multiuser detection. Also, pattern division multiple access (PDMA) [10] attempted to enable massive connectivity with low complexity through an efficient pattern matrix design and a recursive approach of multiuser detection [11]. For a survey on existing works of code-domain NOMA, readers are referred to [5]. Recently, the state-of-the-art technique of deep learning [12] has been applied for multiuser detection in uplink code-domain NOMA systems [13]–[15].

Grant-free access is of tremendous interest to connect a massive number of users to mMTC systems with low latency and low signaling overhead [16]. In uplink grant-free access, active users send their data with no access-grant procedure. Then, a base station (BS) receiver has to identify active users with no aid of a grant procedure and detect each active user's data from the superimposed signal. The principle of compressed sensing (CS) [17] can be applied for multiuser detection in uplink grant-free access, exploiting the sparse activity that many users are present in a cell, but only a few of them are active at a time. Many research articles [18]–[32] demonstrated that a CS-based detector can be successfully deployed at BS for joint activity detection, channel estimation, and/or data detection in uplink grant-free access.

For non-orthogonal and grant-free access, it is crucial to design a set of non-orthogonal sequences with low correlation, constructively or algorithmically, which ultimately guarantees reliable CS-based detection at BS. Moreover, if the transmitted signals of active users are spread onto multiple subcarriers, the high peak-to-average power ratio (PAPR) will cause signal distortion deteriorating all potential benefits of multicarrier communications [33], [34]. Various reduction techniques [34] have been proposed for mitigating the PAPR of multicarrier transmitted signals. Recently, efforts have been made to reduce the PAPR of uplink multicarrier signals in SCMA [35], [36]. In summary, we need to design a set of non-orthogonal sequences with low correlation and low PAPR properties, which ensures reliable and power efficient uplink grant-free access.

In literature, many constructive designs have been presented to provide a variety of pilot or spreading sequences for multiple access. In [37], quasi-orthogonal sequences have been introduced to increase the system capacity of CDMA. Random sequences with the Gaussian distributed elements have been

This work has been submitted to the IEEE for possible publication. Copyright may be transferred without notice, after which this version may no longer be accessible. This work was supported by the National Research Foundation of Korea (NRF) grant funded by the Korea Government (MSIT) (NRF-2021R1F1A1046282).

The author is with the School of of Electrical Engineering and Computer Science (EECS), Gwangju Institute of Science and Technology (GIST), Korea. (e-mail: nyu@gist.ac.kr).

used in [21]–[25] to theoretically guarantee reliable CS-based detection for uplink access. Also, the works of [26]–[30] used pseudo-random noise sequences for CS-based detection in uplink grant-free NOMA. In multicarrier communications, Golay complementary sequences and sets [38]–[40] can be employed to provide theoretically bounded low PAPR. In [41], Golay complementary sequences have been also applied for low PAPR preambles in the filter-bank multicarrier (FBMC) modulation. Binary [42] and non-binary [43] Golay spreading sequences have been employed for low PAPR in uplink grant-free NOMA. Other complementary sequences have been studied in [44]–[48] for PAPR reduction. Zadoff-Chu (ZC) sequences [49], also known as constant amplitude and zero autocorrelation (CAZAC) sequences, have been adopted as preambles for random access in 3GPP-LTE [50], providing low PAPR for multicarrier transmission.

Noting that a sensing matrix of CS is a collection of non-orthogonal column sequences, we can find many algorithmic approaches for good sequences from the efforts of optimizing the sensing matrix. Elad [51] launched an algorithmic design for a sensing matrix by minimizing the average measure of the coherence iteratively. In [52]–[55], several algorithms have been proposed for optimizing a sensing matrix, where each one attempts to approximate its Gram matrix to that of an equiangular tight frame (ETF) [56]. In [57], Chen *et al.* demonstrated that a unit-norm tight frame is a closest design of a nearly orthogonal matrix. Other algorithms can be found in [58] and [59]. From these efforts, each sensing matrix optimized algorithmically can offer a set of non-orthogonal sequences for reliable CS-based detection. In [60] and [61], deep learning (DL) techniques have been also applied for pilot or spreading sequence design. In general, the non-orthogonal sequences obtained by algorithmic and DL-based designs can take arbitrary elements with no structure, which may not be suitable for cost efficient implementation in mMTC devices.

Recently, the genetic algorithm (GA) [62] has been applied for sensing matrix optimization in specific applications, e.g., reducing the complexity of radar imaging [63], allocating an optimized pilot pattern for channel estimation [64], and maximizing the energy efficiency of wireless sensor networks (WSN) [65]. In particular, GA has been used to find subsampling patterns to optimize partial Fourier matrices with specific parameters [63], [64]. This GA-based optimization motivates us to scrutinize the effectiveness of GA for optimizing a sensing matrix, which can ultimately present a set of non-orthogonal sequences for uplink grant-free access.

In this paper, we propose a two-stage genetic algorithm (GA) to design a new set of non-orthogonal sequences¹ for uplink grant-free access, where each sequence has unimodular and complex-valued elements of finite phase for cost efficient implementation in an mMTC device. Each stage of GA makes an evolutionary approach to reach an optimized result by transforming and improving the intermediate outcomes. The first-stage GA is to find a subsampling index set to optimize² a

partial unitary matrix by approximating it to an ETF, where the evolutionary approach tries to minimize the average distance between the inner product of its column pair and the Welch bound equality [66]. Then, the second-stage GA tries to find a sequence to be commonly masked to each column of the partial unitary matrix from the first-stage, in order to reduce the PAPR of the resulting columns. Note that masking each column with a common sequence does not change the inner products and their distribution among the resulting column pairs. Finally, the masked columns of the partial unitary matrix are proposed as new non-orthogonal sequences with low correlation and low PAPR properties, which can be uniquely assigned to users for uplink grant-free access.

Through simulations, the phase transition diagrams reveal that the partial Fourier and ZC-based matrices optimized by our first-stage GA guarantee more reliable CS reconstruction than the randomly subsampled counterparts, respectively, over a wide range of compression and sparsity ratios. In addition, it turns out that the second-stage GA is effective to enhance the PAPR properties of the resulting sequences, where the PAPR distributions appear to be acceptable for multicarrier transmission. In uplink grant-free access, we show that the performance of the Fourier- and ZC-based sequences from our two-stage GA is superior to that of random sequences, while comparable to that of ZC sequences of prime length, for CS-based joint activity detection and channel estimation. Compared to algebraic design, we confirm that this GA-based design can present a new set of non-orthogonal sequences of arbitrary length, exhibiting acceptable PAPR distribution and guaranteeing reliable CS-based detection, which can be more suitable for grant-free massive connectivity.

This paper is organized as follows. Section II describes a system model of uplink grant-free access under consideration, where a CS problem is formulated for joint activity detection and channel estimation. Section III outlines a framework for non-orthogonal sequence design using a two-stage GA. In each stage, we formulate the design goal by an optimization problem. Section IV describes the evolution steps of each stage GA along with the cost function for the optimization problem. Algorithms 1 and 2 summarize the two-stage GA. Section V presents simulation results to demonstrate the effectiveness of each stage GA. In addition, we evaluate the performance of the proposed sequences, comparing to other conventional ones, in CS-based joint activity detection and channel estimation. Finally, concluding remarks will be given in Section IV.

Notations: Throughout this paper, $\mathbb{Z}_N = \{0, \dots, N-1\}$. A matrix (or a vector) is represented by a bold-face upper (or a lower) case letter. \mathbf{X}^T denotes the transpose of a matrix \mathbf{X} , while \mathbf{X}^* is its conjugate transpose. The identity matrix is denoted by \mathbf{I} , where the dimension is determined in the context. $\text{abs}(\mathbf{X}) = [|X_{i,j}|]$ denotes a matrix taking the magnitude of each element of $\mathbf{X} = [X_{i,j}]$. For a vector \mathbf{h} , $\mathbf{h}_{\mathcal{S}}$ is its subvector, indexed by an index set \mathcal{S} , and $\text{diag}(\mathbf{h})$ is a diagonal matrix whose diagonal entries are from \mathbf{h} . The inner product of vectors \mathbf{x} and \mathbf{y} is denoted by $\langle \mathbf{x}, \mathbf{y} \rangle$. The l_2 -norm of a vector $\mathbf{x} = (x_1, \dots, x_N)$ is denoted by $\|\mathbf{x}\|_2 = \sqrt{\sum_{k=1}^N |x_k|^2}$. The Frobenius norm of a matrix

¹The resulting sequences from our design can be used as spreading, pilot, or signature sequences, depending on specific access schemes.

²In this paper, ‘optimize’ does not mean to find a global optimum, since GA may converge to local optima.

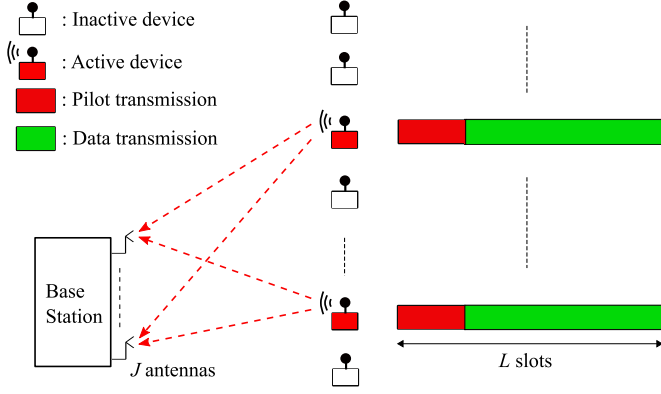


Fig. 1. Two-phase grant-free access scheme with multiple receiver antennas.

$\mathbf{X} = [X_{i,j}]$ is denoted by $\|\mathbf{X}\|_F = \sqrt{\sum_{i,j} |X_{i,j}|^2}$. Finally, $\mathbf{h} \sim \mathcal{CN}(\mathbf{m}, \Sigma)$ is a circularly symmetric complex Gaussian random vector with mean \mathbf{m} and covariance Σ .

II. SYSTEM MODEL

In this paper, we consider a two-phase grant-free access scheme [21], [22] for a single-cell massive connectivity. In an mMTC cell, a base station (BS) receiver equipped with J antennas accommodates total N devices each of which transmits with a single antenna. For a fully grant-free access, we assume that devices are *static*³ in a cell and thus BS accommodates a fixed set of devices having their own user-specific sequences. In the first phase, each active device transmits its sequence as a dedicated pilot, and the BS receiver then tries to identify active devices and estimate their channel profiles from the superimposed pilots. Data can be directly transmitted in the second-phase from active devices with no grant from BS. In this two-phase scheme, we assume that the channels and the device activity remain unchanged during L slots for pilot and data transmissions. Figure 1 illustrates this system model.

With sparse activity, each device is assumed to be active with probability p_a in an i.i.d. manner, where active devices are synchronized. In an access time, an activity indicator vector can be defined by $\boldsymbol{\alpha} = (\alpha_1, \dots, \alpha_N)^T$ with

$$\alpha_n = \begin{cases} 1, & \text{if device } n \text{ is active,} \\ 0, & \text{otherwise,} \end{cases}$$

where $\mathcal{S} = \{n \mid \alpha_n = 1\}$ is a set of active devices and the number of active devices is $|\mathcal{S}| = \sum_{n=1}^N \alpha_n = K \ll N$.

When device n is active, it transmits its unique pilot sequence $\mathbf{s}_n = (s_{1,n}, \dots, s_{M,n})^T$ over M subcarriers for grant-free access, where $M < N$. We consider a flat Rayleigh fading channel, where the channel gain remains unchanged during the coherence time interval of L slots. Let $\mathbf{h}_n = (h_n^{(1)}, \dots, h_n^{(J)})^T$, $1 \leq n \leq N$, be a channel vector from device n , where $h_n^{(t)}$ is the channel gain between device n and BS receiver antenna t . Assuming that the path loss and

³If devices are moving from cell to cell, it is hard to guarantee unique sequence assignment in a fully grant-free manner for all devices in a cell, and some coordination may be required to assign unique sequences to devices.

shadowing effects are known and can be removed by BS, we have $\mathbf{h}_n \sim \mathcal{CN}(\mathbf{0}, \mathbf{I})$. Then, the received signal at antenna t can be represented by

$$\mathbf{y}^{(t)} = \sum_{n=1}^N \alpha_n h_n^{(t)} \mathbf{s}_n + \mathbf{w}^{(t)} = \mathbf{S} \mathbf{x}^{(t)} + \mathbf{w}^{(t)}, \quad (1)$$

where $\mathbf{x}^{(t)} = (\alpha_1 h_1^{(t)}, \dots, \alpha_N h_N^{(t)})^T$ for $1 \leq t \leq J$. In (1), $\mathbf{S} = [\mathbf{s}_1, \dots, \mathbf{s}_N] \in \mathbb{C}^{M \times N}$ is a matrix of pilot sequences, and $\mathbf{w}^{(t)} \sim \mathcal{CN}(\mathbf{0}, \sigma_n^2 \mathbf{I})$ is the complex Gaussian noise vector at antenna t .

Collecting the J received signals of (1), we have a multiple measurement vector (MMV) model of

$$\mathbf{Y} = \mathbf{S} \mathbf{X} + \mathbf{W}, \quad (2)$$

where $\mathbf{Y} = [\mathbf{y}^{(1)}, \dots, \mathbf{y}^{(J)}]$, $\mathbf{X} = [\mathbf{x}^{(1)}, \dots, \mathbf{x}^{(J)}]$, and $\mathbf{W} = [\mathbf{w}^{(1)}, \dots, \mathbf{w}^{(J)}]$, respectively. Due to the activity indicator $\boldsymbol{\alpha}$, it is clear that \mathbf{X} has the row-wise sparsity with K nonzero and $N - K$ zero rows. Then, BS can apply a joint sparse recovery algorithm to solve the MMV problem of (2), in order to detect the activity indicator $\boldsymbol{\alpha}$ and estimate the channel vector \mathbf{h}_n for $n \in \mathcal{S}$. If the nonzero rows of \mathbf{X} are estimated, the row indices mean a detected index set of active devices, denoted by $\hat{\mathcal{S}}$, while the coefficients of each nonzero row give an estimated channel vector $\hat{\mathbf{h}}_n$ for $n \in \hat{\mathcal{S}}$. The CS-based joint active user detection (AUD) and channel estimation (CE) complete the first phase of uplink grant-free access. In the second phase, the BS receiver detects data from active devices with the knowledge of device identity and channel profiles obtained from the first phase [21], [22]. In this paper, we restrict our attention to joint AUD and CE in the first phase via joint sparse recovery under the CS MMV model.

Remark 1: A CS MMV model can also be applied for *one-shot* detection in uplink grant-free NOMA [29], [42]. In this system, each active device transmits its unique spreading sequence of length M , spread onto M subcarriers, carrying its pilot and data over J time slots. Assuming that the channels and the device activity remain unchanged, the received signals over J slots are also modeled by (2). A BS receiver equipped with a single antenna then conducts CS-based joint activity detection, channel estimation, and data detection, by solving the MMV problem of (2). Readers are referred to [29] and [42] for more details.

III. FRAMEWORK FOR SEQUENCE DESIGN

The goal of this paper is to present a set of non-orthogonal sequences for grant-free massive connectivity. In CS MMV model, the sequence set forms the matrix \mathbf{S} in (2), where the problem of sequence design boils down to designing a sensing matrix for reliable CS-based detection. This section outlines a framework for sensing matrix design using the genetic algorithm (GA), which ultimately provides a set of good non-orthogonal sequences for uplink grant-free access.

A. Partial Unitary Matrices

Compressed sensing (CS) [17] is to reconstruct an N -dimensional sparse signal \mathbf{x} from its underdetermined M -dimensional measurement $\mathbf{y} = \mathbf{A} \mathbf{x}$, where $M < N$. The

signal \mathbf{x} is called K -sparse if it has at most K nonzero elements, where $K \ll N$. In CS techniques, it is essential to design a good $M \times N$ sensing matrix \mathbf{A} , in order to guarantee reliable reconstruction of sparse signals.

Taking some rows out of a unitary matrix is a well known operation to obtain a *partial* unitary matrix [67] that enjoys practical benefits as well as theoretical CS recovery guarantee. A partial unitary matrix is formulated by

$$\mathbf{A} = \frac{1}{\sqrt{M}} \mathbf{R}_\Omega \mathbf{U} \triangleq \mathbf{U}_\Omega, \quad (3)$$

where \mathbf{U} is an $N \times N$ unitary matrix of $\mathbf{U}\mathbf{U}^* = \mathbf{U}^*\mathbf{U} = \mathbf{N}\mathbf{I}$. In (3), \mathbf{R}_Ω is a subsampling operator selecting M rows out of N ones whose indices are specified by $\Omega \subset \{1, \dots, N\}$, where $|\Omega| = M$. If the indices of Ω are selected randomly, $\mathbf{A} = \mathbf{U}_\Omega$ guarantees reliable CS reconstruction theoretically with high probability, provided that $M \geq \mathcal{O}(K \log^4 N)$ [68]. In practice, a partial unitary matrix allows fast and efficient measurement and reconstruction for CS, thanks to the fast unitary transform, e.g., fast Fourier or Hadamard transform.

To design unimodular sequences, we begin with a unitary matrix \mathbf{U} whose elements take the magnitude of 1. Then, the first stage of sequence design attempts to find a subsampling index set Ω to optimize a partial unitary matrix \mathbf{U}_Ω for reliable CS reconstruction.

B. PAPR Reduction

In system model of Section II, if the sequence \mathbf{s}_n is transmitted through M subcarriers, the peak-to-average power ratio (PAPR) of its OFDM signal is determined by [33]

$$\text{PAPR}(\mathbf{s}_n) = \max_{t \in [0,1)} \frac{\left| \sum_{i=1}^M s_{m,n} e^{j2\pi(m-1)t} \right|^2}{M}, \quad (4)$$

where $j = \sqrt{-1}$. In (4), we assumed that \mathbf{s}_n is unimodular, i.e., $|s_{m,n}| = 1$, for $m = 1, \dots, M$.

Given a partial unitary matrix \mathbf{U}_Ω , we try to reduce the PAPR of the column sequences⁴. For PAPR reduction, we apply a unimodular and complex-valued sequence $\mathbf{v} = (v_1, \dots, v_M)^T$ as a common mask to each column of \mathbf{U}_Ω , i.e.,

$$\mathbf{U}_{\Omega, \mathbf{v}} = \text{diag}(\mathbf{v}) \cdot \mathbf{U}_\Omega. \quad (5)$$

In (5), we use a modulated q -ary sequence for \mathbf{v} , i.e., $v_m = e^{j\frac{2\pi a_m}{q}}$, where $a_m \in \mathbb{Z}_q$ for $m = 1, \dots, M$. Then, it is clear that the inner product of a column pair in $\mathbf{U}_{\Omega, \mathbf{v}}$ is identical to that of the corresponding pair in \mathbf{U}_Ω , since $\mathbf{U}_{\Omega, \mathbf{v}}^* \mathbf{U}_{\Omega, \mathbf{v}} = \mathbf{U}_\Omega^* \mathbf{U}_\Omega$, which suggests that the new matrix $\mathbf{U}_{\Omega, \mathbf{v}}$ may exhibit the same performance of CS-based detection as the matrix \mathbf{U}_Ω .

In the second design stage, we search for a masking sequence \mathbf{v} that allows the column sequences of $\mathbf{U}_{\Omega, \mathbf{v}}$ to have a desired PAPR property, maintaining the performance of reliable CS reconstruction from the first design stage.

⁴If \mathbf{U} has a column of all ones, like the Fourier or Hadamard matrix, the maximum PAPR of the column sequences of its partial unitary matrix \mathbf{U}_Ω has the highest value of M , regardless of Ω .

C. Genetic Algorithm

The genetic algorithm (GA) is an evolutionary technique to solve an optimization problem that is computationally intractable [62]. Inspired by the evolutionary mechanism in nature, GA transforms and evolves *chromosomes* through crossover, mutation, selection, population updates, and so on. Through a sufficient number of generations, GA converges to a fittest chromosome, which can be a solution to the optimization problem. Thanks to the fast convergence to local optima, GA has attracted much attention in machine learning and data mining [69]–[71]. Recently, GA has expanded its application to other areas, e.g., channel coding [72]–[75], spreading code design [76], [77], CS recovery [78]–[80] and matrix optimization [63]–[65], etc.

In Section III.A and III.B, we introduced two design stages to obtain a set of good sequences. At each stage, the design goal can be specified by an optimization problem that needs to be solved by GA. Given a unitary matrix \mathbf{U} , the objective of the first design stage is to find a fittest chromosome or subsampling index set Ω in (3). The optimization problem for this objective can be formulated by

$$\Omega_{\text{opt}} = \underset{\Omega \subset \{1, \dots, N\}, |\Omega|=M}{\text{argmin}} f_1(\mathbf{U}_\Omega), \quad (6)$$

where $f_1(\mathbf{U}_\Omega)$ is a cost function of the first-stage optimization. The cost function needs to be a good metric that reflects the performance of CS reconstruction with the partial unitary matrix \mathbf{U}_Ω . The first-stage GA tries to minimize the cost function $f_1(\mathbf{U}_\Omega)$ through evolution steps, in order to find a solution to (6).

When the first-stage GA is completed, the partial unitary matrix $\mathbf{U}_{\Omega_{\text{opt}}}$ with an optimized subsampling index set Ω_{opt} is available for the second design stage. Given Ω_{opt} , the second-stage GA tries to find a fittest chromosome or unimodular masking sequence \mathbf{v} of length M , which is a solution to another optimization problem of

$$\mathbf{v}_{\text{opt}} = \underset{\mathbf{v} \in \mathcal{V}_{q,M}}{\text{argmin}} f_2(\mathbf{U}_{\Omega_{\text{opt}}, \mathbf{v}}), \quad (7)$$

where $\mathcal{V}_{q,M}$ is a set of all modulated q -ary sequences of length M . In (7), $f_2(\mathbf{U}_{\Omega_{\text{opt}}, \mathbf{v}})$ is a cost function of the second-stage optimization, which should be a metric for the PAPR property of the column sequences of $\mathbf{U}_{\Omega_{\text{opt}}, \mathbf{v}}$. The second-stage GA tries to enhance the PAPR property with \mathbf{v}_{opt} , maintaining the performance of $\mathbf{U}_{\Omega_{\text{opt}}}$ for reliable CS reconstruction.

Finally, if Ω_{opt} and \mathbf{v}_{opt} are found by the two-stage GA, we obtain the matrix $\mathbf{S} = \mathbf{U}_{\Omega_{\text{opt}}, \mathbf{v}_{\text{opt}}}$ in (2), where the column sequences are proposed as non-orthogonal sequences with low PAPR for reliable CS-based detection in uplink grant-free access. In next section, our two-stage GA will be described with the details to find Ω_{opt} and \mathbf{v}_{opt} , respectively.

IV. TWO-STAGE GENETIC ALGORITHM

In this section, we describe the evolutionary steps of our two-stage GA. The first-stage GA is to find an optimized subsampling index set $\Omega_{\text{opt}} \subset \{1, \dots, N\}$ with $|\Omega_{\text{opt}}| = M$, where M and N are fixed. Given Ω_{opt} , the second-stage GA then attempts to find an optimized masking sequence $\mathbf{v}_{\text{opt}} \in \mathcal{V}_{q,M}$, where $q = N$.

A. Stage 1: Subsampling Optimization

1) *Initialization*: A population \mathcal{P}_1 is defined by a collection of T_1 subsampling index sets, i.e., $\mathcal{P}_1 = (\Omega_1, \Omega_2, \dots, \Omega_{T_1})$, where $\Omega_t \subset \{1, \dots, N\}$ with $|\Omega_t| = M$ for $t = 1, \dots, T_1$. Initially, the indices of Ω_t are selected randomly.

2) *Cost Function*: In the first-stage, we propose the cost function for an index set Ω_t by

$$f_1(\mathbf{U}_{\Omega_t}) = \frac{1}{\sqrt{N(N-1)}} \left\| \text{abs}(\mathbf{U}_{\Omega_t}^* \mathbf{U}_{\Omega_t}) - \mathbf{G}_W \right\|_F, \quad (8)$$

where $\mathbf{G}_W \in \mathbb{R}^{N \times N}$ is a matrix with diagonal entries of 1 and off-diagonal entries of $\sqrt{\frac{N-M}{M(N-1)}}$. Intuitively, the cost function of (8) represents the average (rms-sense) distance between the inner product of a column pair of \mathbf{U}_{Ω_t} and the Welch bound equality (WBE) [66]. Attempting to minimize the cost function, the first-stage GA makes the inner product of a column pair of \mathbf{U}_{Ω_t} closer to the WBE, which approximates the resulting matrix to an equiangular tight frame (ETF) [56]. The target matrix \mathbf{G}_W is similar to, but not the same as the one in the convex set (e.g. (12) in [53] and (14) in [54]) for optimizing CS matrices. As remarked by [54], it is more reasonable to measure a distance from \mathbf{G}_W in (8), rather than \mathbf{I} , which has been confirmed by the optimization of [53].

3) *Crossover*: In population \mathcal{P}_1 , let us consider a pair of index sets Ω_{t_1} and Ω_{t_2} , $1 \leq t_1 \neq t_2 \leq T_1$, where we assume $f_1(\mathbf{U}_{\Omega_{t_1}}) < f_1(\mathbf{U}_{\Omega_{t_2}})$. Then, $d_1 = \lceil \beta_1 \cdot M \rceil$ and $d_2 = M - d_1$ indices are randomly selected from Ω_{t_1} and Ω_{t_2} , respectively, where $\beta_1 > 0.5$. Finally, the selected indices, which should be all distinct, are combined to generate a new index set through *crossover*. In other words, we create a new subsampling index set by combining parents, where a parent index set with a lower cost function is more involved in creating its offspring. We apply the crossover for every pair of parent index sets from \mathcal{P}_1 , which yields a new population \mathcal{C}_1 of size $\binom{T_1}{2} = \frac{T_1(T_1-1)}{2}$ at each evolution step.

4) *Mutation*: In nature, parts of a chromosome can be mutated in a generation, which provides diversity for evolution. In the first-stage GA, μ_1 indices are randomly selected from each index set in \mathcal{P}_1 , which is then replaced by new (random) ones through *mutation*. At each evolution step, we apply the mutation to all index sets in \mathcal{P}_1 , which yields a new population \mathcal{M}_1 of size T_1 .

5) *Population Update*: Through crossover and mutation, we have a new, intermediate population $\mathcal{I}_1 = \mathcal{P}_1 + \mathcal{C}_1 + \mathcal{M}_1$, where the size⁵ is $|\mathcal{I}_1| = T_1 + \binom{T_1}{2} + T_1 = \frac{T_1(T_1+3)}{2}$. From \mathcal{I}_1 , we select the T_1 index sets with the T_1 lowest cost functions of (8). The population \mathcal{P}_1 is then updated by the T_1 fittest index sets at each evolution step.

6) *Iteration and Selection*: In the first-stage GA, the evolution steps of crossover, mutation, and population update are repeated by a predefined number of iterations, denoted by $I_{\max,1}$. In the end, the fittest index set of \mathcal{P}_1 , which has the lowest cost function of (8), will be selected as an optimized subsampling index set Ω_{opt} .

Algorithm 1 describes the entire steps of the first-stage GA to optimize a subsampling index set.

⁵Identical chromosomes in \mathcal{I}_1 (or \mathcal{I}_2), if any, are treated as separate ones.

Algorithm 1 Genetic Algorithm for Subsampling Optimization

Input: Unitary matrix \mathbf{U} , Number of measurements M ,

Population size T_1 , Crossover rate β_1 , Mutation rate μ_1 ,

Maximum number of iterations $I_{\max,1}$.

Initialization: Create a population $\mathcal{P}_1 = \{\Omega_1, \dots, \Omega_{T_1}\}$

of randomly selected index sets, where $|\Omega_t| = M$.

Compute the cost function (8) for each index set of \mathcal{P}_1 .

Iteration:

for $i = 1$ to $I_{\max,1}$ **do**

Crossover: Create a new population \mathcal{C}_1 with index sets from \mathcal{P}_1 .

Mutation: Create a new population \mathcal{M}_1 with index sets from \mathcal{P}_1 .

Population update: Compute the cost function (8) for each index set of $\mathcal{I}_1 = \mathcal{P}_1 + \mathcal{C}_1 + \mathcal{M}_1$, select the T_1 index sets from \mathcal{I}_1 with the T_1 lowest cost functions, and update \mathcal{P}_1 with the T_1 fittest index sets.

end for

Selection: Select the fittest index set Ω_{opt} from \mathcal{P}_1 .

Output: Optimized subsampling index set Ω_{opt}

B. Stage 2: Masking Sequence Optimization

1) *Initialization*: In the second-stage GA, a population consists of T_2 masking sequences, i.e., $\mathcal{P}_2 = (\mathbf{v}_1, \dots, \mathbf{v}_{T_2})$, where each element of $\mathbf{v}_t = (v_{1,t}, \dots, v_{M,t})^T$ is $v_{m,t} = e^{j \frac{2\pi a_{m,t}}{N}}$ for $m = 1, \dots, M$ and $t = 1, \dots, T_2$. Initially, $a_{m,t}$ is randomly taken from \mathbb{Z}_N .

2) *Cost Function*: Note that the partial unitary matrix $\mathbf{U}_{\Omega_{\text{opt}}}$ is available by the optimized subsampling index set Ω_{opt} from the first-stage GA. In the second-stage GA, the cost function for a masking sequence \mathbf{v}_t is proposed by

$$f_2(\mathbf{U}_{\Omega_{\text{opt}}, \mathbf{v}_t}) = \frac{1}{|\mathcal{K}_\delta|} \sum_{\mathbf{p}_n \in \mathcal{K}_\delta} \text{PAPR}(\mathbf{p}_n), \quad (9)$$

where $\mathbf{U}_{\Omega_{\text{opt}}, \mathbf{v}_t} = \text{diag}(\mathbf{v}_t) \cdot \mathbf{U}_{\Omega_{\text{opt}}} = [\mathbf{p}_1, \dots, \mathbf{p}_N] \triangleq \mathbf{P}$. In (9), \mathcal{K}_δ is a set of columns in \mathbf{P} whose PAPR belong to the top $\delta\%$, where $|\mathcal{K}_\delta| = \lfloor \frac{\delta N}{100} \rfloor$. That is, $f_2(\mathbf{U}_{\Omega_{\text{opt}}, \mathbf{v}_t})$ is the average of top $\delta\%$ PAPR of \mathbf{P} , which will be minimized to enhance the PAPR distribution of the columns of \mathbf{P} .

3) *Crossover*: As in the first-stage GA, we consider a pair of sequences \mathbf{v}_{t_1} and \mathbf{v}_{t_2} from \mathcal{P}_2 , $1 \leq t_1 \neq t_2 \leq T_2$, where $f_2(\mathbf{U}_{\Omega_{\text{opt}}, \mathbf{v}_{t_1}}) < f_2(\mathbf{U}_{\Omega_{\text{opt}}, \mathbf{v}_{t_2}})$. Then, the first $d_1 = \lceil \beta_2 \cdot M \rceil$ elements from \mathbf{v}_{t_1} and the last $d_2 = M - d_1$ elements from \mathbf{v}_{t_2} are combined to generate a new masking sequence, where $\beta_2 > 0.5$. Applying the crossover for every pair of sequences in \mathcal{P}_2 , we have a new population \mathcal{C}_2 of size $\binom{T_2}{2} = \frac{T_2(T_2-1)}{2}$ at each evolution step.

4) *Mutation*: For mutation, the second-stage GA randomly selects μ_2 elements from each sequence in \mathcal{P}_2 , where each element is replaced by a new (random) N -ary modulated one. We obtain a new population \mathcal{M}_2 of size T_2 by applying the mutation to all sequences in \mathcal{P}_2 .

5) *Population Update*: Through crossover and mutation, we obtain $\mathcal{I}_2 = \mathcal{P}_2 + \mathcal{C}_2 + \mathcal{M}_2$, where $|\mathcal{I}_2| = \frac{T_2(T_2+3)}{2}$. From \mathcal{I}_2 , we select the T_2 sequences with the T_2 lowest cost functions of (9). The population \mathcal{P}_2 is then updated by the T_2 fittest sequences at each evolution step.

6) *Iteration and Selection*: In the second-stage GA, crossover, mutation, and population update are repeated by a predefined number of iterations, denoted by $I_{\max,2}$. Finally, the fittest sequence of \mathcal{P}_2 , which has the lowest cost function of (9), will be selected as an optimized mask \mathbf{v}_{opt} .

Algorithm 2 Genetic Algorithm for Masking Sequence Optimization

Input: Partial unitary matrix $\mathbf{U}_{\Omega_{\text{opt}}}$, Number of measurements M , Population size T_2 , Crossover rate β_2 , Mutation rate μ_2 , Maximum number of iterations $I_{\text{max},2}$.

Initialization: Create a population $\mathcal{P}_2 = \{\mathbf{v}_1, \dots, \mathbf{v}_{T_2}\}$ of random modulated N -ary sequences of length M . Compute the cost function (9) for each sequence of \mathcal{P}_2 .

Iteration:

for $i = 1$ to $I_{\text{max},2}$ **do**

Crossover: Create a new population \mathcal{C}_2 with sequences from \mathcal{P}_2 .

Mutation: Create a new population \mathcal{M}_2 with sequences from \mathcal{P}_2 .

Population update: Compute the cost function (9) for each sequence of $\mathcal{I}_2 = \mathcal{P}_2 + \mathcal{C}_2 + \mathcal{M}_2$, select the T_2 sequences from \mathcal{I}_2 with the T_2 lowest cost functions, and update \mathcal{P}_2 with the T_2 fittest sequences.

end for

Selection: Select the fittest masking sequence \mathbf{v}_{opt} from \mathcal{P}_2 .

Output: Optimized masking sequence \mathbf{v}_{opt}

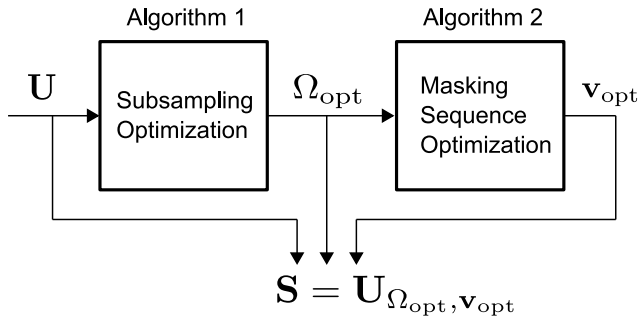


Fig. 2. Two-stage GA for non-orthogonal sequence design.

Algorithm 2 describes the entire steps of the second-stage GA to optimize a masking sequence. Finally, a set of non-orthogonal sequences, or $\mathbf{S} = \mathbf{U}_{\Omega_{\text{opt}}, \mathbf{v}_{\text{opt}}}$, is provided by our two-stage GA of Algorithms 1 and 2, as illustrated by Fig. 2.

Remark 2: The set of non-orthogonal sequences designed by our two-stage GA can be represented by

$$\mathbf{S} = \mathbf{U}_{\Omega_{\text{opt}}, \mathbf{v}_{\text{opt}}} = \frac{1}{\sqrt{M}} \text{diag}(\mathbf{v}_{\text{opt}}) \cdot \mathbf{R}_{\Omega_{\text{opt}}} \mathbf{U}. \quad (10)$$

Given a unitary matrix \mathbf{U} , (10) means that the matrix \mathbf{S} can be generated by the operations of row selection specified by Ω_{opt} and masking by \mathbf{v}_{opt} . Therefore, a BS receiver can generate the sequence set \mathbf{S} easily with the highly structured unitary matrix \mathbf{U} by storing Ω_{opt} and \mathbf{v}_{opt} . Moreover, CS-based detection can be carried out fast and efficiently at BS, exploiting the fast unitary transform by \mathbf{U} . Also, each mMTC device is able to generate its unique sequence on-the-fly with a unique column structure of \mathbf{U} by storing Ω_{opt} and \mathbf{v}_{opt} , which allows its cheap and efficient implementation.

V. SIMULATION RESULTS

In this section, we first demonstrate the effectiveness of our two-stage GA for non-orthogonal sequence design. Then, we present simulation results of CS-based detection for uplink grant-free access, which demonstrates the performance of non-orthogonal sequences designed by our two-stage GA.

For the unitary matrix \mathbf{U} , we use the $N \times N$ Fourier matrix $\mathbf{F} = [F_{k,l}]$, where $F_{k,l} = e^{-j\frac{2\pi(k-1)(l-1)}{N}}$ for $1 \leq k, l \leq N$.

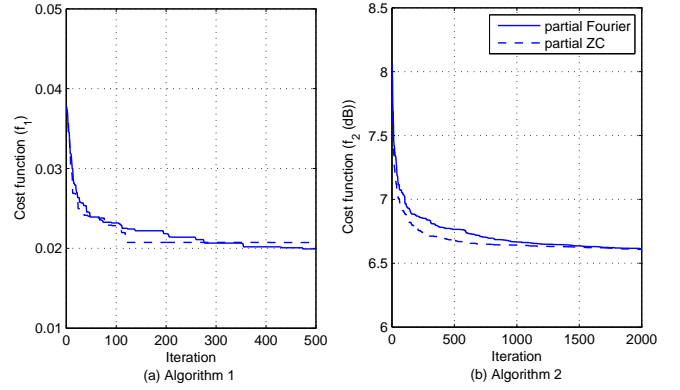


Fig. 3. Evolution of the cost functions of Algorithms 1 and 2, where $N = 256$ and $M = 80$. Each curve shows the cost function of the fittest chromosome at each iteration.

Additionally, we consider another unitary matrix based on Zadoff-Chu (ZC) sequences [49]. Each cyclic shift of the ZC sequence of even length becomes a column of a matrix $\mathbf{Z} = [Z_{k,l}]$, where each element is given by

$$Z_{k,l} = e^{-j\frac{\pi(k+N-l)^2}{N}}, \quad 1 \leq k, l \leq N.$$

Due to the perfect auto-correlation [49] of ZC sequences, it is clear that \mathbf{Z} , called the ZC matrix, is also unitary.

Beginning with \mathbf{F} and \mathbf{Z} , our two-stage GA gives $\mathbf{F}_{\Omega_{\text{opt}}, \mathbf{v}_{\text{opt}}}$ and $\mathbf{Z}_{\Omega_{\text{opt}}, \mathbf{v}_{\text{opt}}}$, respectively, by Algorithms 1 and 2. Finally, their columns are proposed as non-orthogonal sequences, called *Fourier-based* and *ZC-based* sequences, respectively.

A. Effectiveness of Two-Stage GA

In simulations, each stage GA has the population size of $T_1 = T_2 = 20$, the crossover rate $\beta_1 = \beta_2 = 0.7$, and the mutation number $\mu_1 = \mu_2 = 1$, respectively. Algorithm 1 has $I_{\text{max},1} = 500$, whereas $I_{\text{max},2} = 2000$ in Algorithm 2, as experiments showed that the cost function of Algorithm 2 converges slowly. Finally, the cost function of Algorithm 2 computes top $\delta = 30\%$ average of PAPR of $\mathbf{P} = \mathbf{F}_{\Omega_{\text{opt}}, \mathbf{v}_{\text{opt}}}$ (or $\mathbf{Z}_{\Omega_{\text{opt}}, \mathbf{v}_{\text{opt}}}$) for a mask sequence \mathbf{v}_t .

Fig. 3 displays the evolution of the cost functions (8) and (9) of the fittest chromosomes, respectively, from $M \times N$ partial Fourier and ZC matrices, where $N = 256$ and $M = 80$. The figure shows that each stage GA continues to reduce its cost function over the evolution steps. As mentioned above, we observed that the cost function of Algorithm 2 converges slowly, compared to that of Algorithm 1. It is because the search space size for the optimization problem (7) is N^M , which is much larger than that of (6), or $\binom{N}{M} \leq \left(\frac{eN}{M}\right)^M$. Fig. 3 also reveals that the cost functions of partial Fourier and ZC matrices converge to similar values, which suggests that their performance of CS reconstruction and PAPR property will be similar to each other.

To investigate the effectiveness of the first-stage GA, we sketch the phase transition diagrams for CS reconstruction with partial Fourier and ZC matrices, respectively, obtained by Algorithm 1. We consider an MMV problem $\mathbf{Y} = \mathbf{A}\mathbf{X} + \mathbf{W}$, where $\mathbf{A} = \mathbf{F}_{\Omega_{\text{opt}}}$ (or $\mathbf{Z}_{\Omega_{\text{opt}}}$), $\mathbf{X} = (\mathbf{x}_1, \dots, \mathbf{x}_J)$ is a

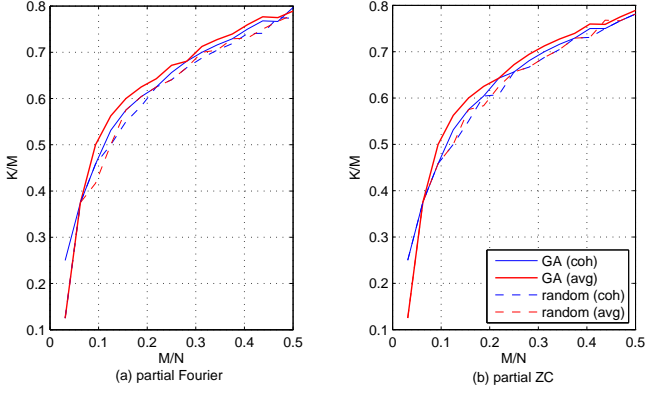


Fig. 4. Phase transitions for partial Fourier and ZC matrices under MMV reconstruction (SOMP), where $N = 256$ and $J = 8$ at SNR = 20 dB.

jointly sparse matrix with common nonzero rows, and $\mathbf{Y} = (\mathbf{y}_1, \dots, \mathbf{y}_J)$ is a collection of $J = 8$ measurement vectors. The nonzero entries of \mathbf{X} are independently drawn from $\mathcal{CN}(0, 1)$, where their row positions are uniformly distributed. Also, each element of \mathbf{W} is the i.i.d. Gaussian noise from $\mathcal{CN}(0, \sigma_n^2)$, where the signal-to-noise ratio (SNR) is set to $\text{SNR} = \frac{\sum_{i=1}^J \|\mathbf{A}\mathbf{x}_i\|_2^2}{JKM\sigma_n^2} = 20$ dB. In phase transition, we made 10^4 trials of CS reconstruction at each test point, where the step sizes of $\frac{M}{N}$ and $\frac{K}{M}$ are 2^{-5} and 10^{-2} , respectively. The phase transition indicates that the corresponding CS reconstruction is successful with probability exceeding 99% below the transition curve, where a success is declared if an estimated $\hat{\mathbf{X}}$ achieves $\frac{\|\mathbf{X} - \hat{\mathbf{X}}\|_F^2}{\|\mathbf{X}\|_F^2} < 10^{-2}$.

Fig. 4 depicts the phase transitions for partial Fourier and ZC matrices under MMV reconstruction by the simultaneous orthogonal matching pursuit (SOMP) [81], where the number of nonzero rows of \mathbf{X} is assumed to be known in advance. In the figure, ‘GA (avg)’ indicates the phase transition of $\mathbf{F}_{\Omega_{\text{opt}}}$ (or $\mathbf{Z}_{\Omega_{\text{opt}}}$) for which the cost function (8) has been minimized by Algorithm 1. Meanwhile, ‘GA (coh)’ corresponds to the case in which Algorithm 1 changed its cost function with the mutual coherence, i.e., $f_1(\mathbf{U}_{\Omega_t}) = \max_{1 \leq k \neq l \leq N} \frac{|(\mathbf{a}_k, \mathbf{a}_l)|}{\|\mathbf{a}_k\|_2 \|\mathbf{a}_l\|_2}$, where \mathbf{a}_k and \mathbf{a}_l are the k th and the l th columns of $\mathbf{A} = \mathbf{U}_{\Omega_t}$, respectively, with $\mathbf{U} = \mathbf{F}$ or \mathbf{Z} . Also, ‘random (coh)’ and ‘random (avg)’ show the phase transitions for randomly subsampled Fourier (or ZC) matrices that have the lowest coherence and the lowest cost function (8), respectively, out of 500 trials. Fig. 4 shows that the phase transition curves of ‘GA (avg)’ are higher than or equal to all the other ones over most compression ratios, which demonstrates that the partial Fourier and ZC matrices optimized by Algorithm 1 with the cost function (8) present reliable MMV reconstruction over a wide range of compression ($\frac{M}{N}$) and sparsity ($\frac{K}{M}$) ratios.

The effectiveness of the second-stage GA is verified by Fig. 5, which sketches the maximum and top 30% average PAPR of the sequences obtained by Algorithm 2. In the figure, ‘avg’ means that Algorithm 2 utilized the cost function of (9), while ‘max’ indicates that the maximum PAPR of $\mathbf{U}_{\Omega_{\text{opt}}, \mathbf{v}_t}$ has been used as the cost function of Algorithm 2, where $\mathbf{U} = \mathbf{F}$ or \mathbf{Z} . To demonstrate the PAPR improvement by Algorithm 2,

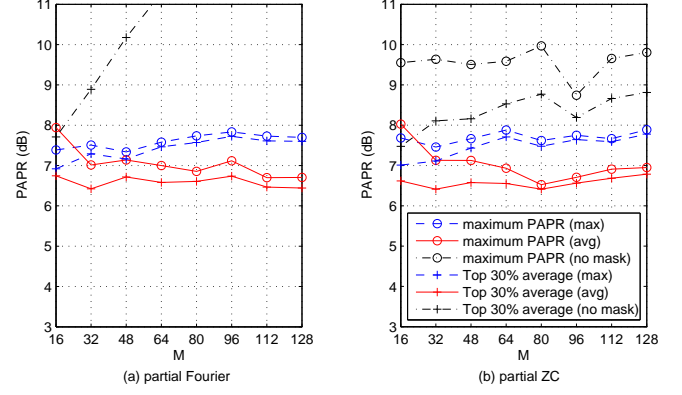


Fig. 5. Maximum and top 30% average PAPR of non-orthogonal sequences from partial Fourier and ZC matrices, where $N = 256$.

we also sketch ‘no mask’, which indicates the PAPR properties of the sequences obtained by Algorithm 1 only, or column sequences of $\mathbf{F}_{\Omega_{\text{opt}}}$ (or $\mathbf{Z}_{\Omega_{\text{opt}}}$). Note that the maximum PAPR of partial Fourier matrices for ‘no mask’ is outside the scope of this figure, taking the highest value of M due to a column of all ones in $\mathbf{F}_{\Omega_{\text{opt}}}$. Fig. 5 demonstrates that Algorithm 2 can significantly reduce the maximum and top 30% average PAPR of the sequences from $\mathbf{F}_{\Omega_{\text{opt}}}$ and $\mathbf{Z}_{\Omega_{\text{opt}}}$, respectively. Also, it reveals that using the cost function (9) is more effective for Algorithm 2 to enhance the PAPR properties.

B. Performance of CS-based Detection

Numerical experiments examine the performance of the proposed non-orthogonal sequences for CS-based AUD and CE in uplink grant-free access. Under the system model of Section II, we assume that there are $N = 500$ devices in an mMTC cell, where each one is assigned a unique non-orthogonal pilot sequence of length $M = 80$. Reflecting sparse activity, each device sends its pilot with probability $p_a = 0.1$ at each access time. At BS, the received signal-to-noise ratio (SNR) per device is set to $\text{SNR} = \frac{1}{K} \cdot \frac{\sum_{i=1}^J \|\mathbf{S}\mathbf{x}^{(i)}\|_2^2}{JM\sigma_n^2}$.

For CS-based AUD and CE, a BS receiver deploys the SOMP algorithm that requires no prior knowledge of the number of active devices⁶. In AUD, both undetected and false-alarmed devices are treated as errors. Thus, the activity error rate (AER) is defined by the average of $\frac{|\mathcal{S} \setminus \hat{\mathcal{S}}| + |\hat{\mathcal{S}} \setminus \mathcal{S}|}{|\mathcal{S} \cup \hat{\mathcal{S}}|}$, where \mathcal{S} and $\hat{\mathcal{S}}$ are true and detected sets of active devices, respectively. Also, channel estimation errors are measured by the normalized mean squared errors (NMSE), or the average of $\frac{\|\mathbf{h}_{\mathcal{S}} - \hat{\mathbf{h}}_{\mathcal{S}}\|_2^2}{\|\mathbf{h}_{\mathcal{S}}\|_2^2}$, where $\mathbf{h}_{\mathcal{S}}$ and $\hat{\mathbf{h}}_{\mathcal{S}}$ are true and estimated channel vectors, respectively, for truly active devices. In simulations, the averages for AER and NMSE are computed over 10^4 access trials.

To obtain the Fourier- and ZC-based sequences from $\mathbf{F}_{\Omega_{\text{opt}}, \mathbf{v}_{\text{opt}}}$ and $\mathbf{Z}_{\Omega_{\text{opt}}, \mathbf{v}_{\text{opt}}}$, respectively, Algorithms 1 and 2 use the same parameters as in Section V.A, but $I_{\text{max}, 1} = 1000$ and $I_{\text{max}, 2} = 4000$. For comparison, we generate complex-valued random Gaussian sequences of length M , where each

⁶In simulations, this sparsity-blind SOMP stops its iteration empirically if the maximum signal proxy is less than $\sqrt{3\sigma_n^2 J}$.

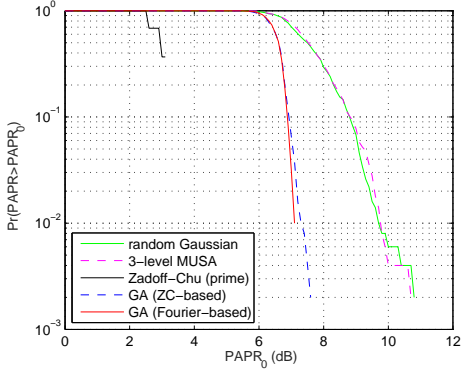


Fig. 6. PAPR distribution (CCDF) of non-orthogonal sequences of length $M = 80$ ($M_{ZC} = 79$), where $N = 500$.

element is drawn from the i.i.d. complex Gaussian distribution with zero mean and variance $1/M$ [21]. Also, we use the complex-valued MUSA spreading sequences of length M , where each element is randomly taken from the 3-level signal constellation, i.e., $\frac{1}{\sqrt{12}}[\pm 1 \pm j, \pm 1, \pm j, 0]$, in Fig. 2(b) of [9]. Generating N random Gaussian and N MUSA sequences, we have $M \times N$ matrices \mathbf{G} and \mathbf{M} , respectively, where each one is a matrix with the lowest coherence among 1000 trials.

The last sequence set for comparison is obtained by cyclic shifts of the Zadoff-Chu (ZC) sequences with multiple roots, where the sequence length $M_{ZC} = 79$ is a prime number closest to M . In specific, we begin with an $M_{ZC} \times M_{ZC}$ matrix \mathbf{C}_u that consists of all cyclic shifts of a u th root ZC sequence [49] of length M_{ZC} with the k th element of $e^{\frac{j\pi u k(k+1)}{M_{ZC}}}$, where u is a root number between 1 and $M_{ZC} - 1$. Due to the perfect autocorrelation of the ZC sequence, \mathbf{C}_u is unitary for any u . For a set of sequences with low PAPR, we then sort the root numbers $u = 1, \dots, M_{ZC} - 1$ in ascending order of the maximum PAPR that the column sequences of \mathbf{C}_u achieve. Taking the first $L = \lceil \frac{N}{M_{ZC}} \rceil$ root numbers, denoted by u_1, \dots, u_L , we produce a matrix $\mathbf{C}' = [\mathbf{C}_{u_1}, \dots, \mathbf{C}_{u_L}]$, where the first N columns are finally selected for an $M_{ZC} \times N$ matrix \mathbf{C} , or a set of ZC sequences of prime length M_{ZC} . The coherence of \mathbf{C} is $\frac{1}{\sqrt{M_{ZC}}}$, close to the Welch bound equality, due to the cross-correlation of ZC sequences with distinct roots [82]. In simulations, the matrix \mathbf{S} in (2) is determined by the sequence sets under consideration, i.e., $\mathbf{S} = \mathbf{F}_{\Omega_{\text{opt}}, \mathbf{v}_{\text{opt}}}, \mathbf{Z}_{\Omega_{\text{opt}}, \mathbf{v}_{\text{opt}}}, \mathbf{G}, \mathbf{M}$, and \mathbf{C} , respectively.

Fig. 6 displays the complementary cumulative distribution function (CCDF) of PAPR of non-orthogonal sequences under consideration, where $N = 500$ and $M = 80$ ($M_{ZC} = 79$). The ZC sequences of prime length M_{ZC} , whose PAPR has been optimized as mentioned above, exhibit the best PAPR distribution with maximum of 3.14 dB. On the other hand, complex-valued random Gaussian and MUSA sequences have the poor distributions, where the maximum PAPR are 10.86 dB and 10.79 dB, respectively. It is shown that the PAPR distributions of Fourier- and ZC-based sequences from our two-stage GA are not so good as that of ZC sequences of prime length, but much better than those of the random sequences, showing the maximum of 7.18 dB and 7.66 dB, respectively.

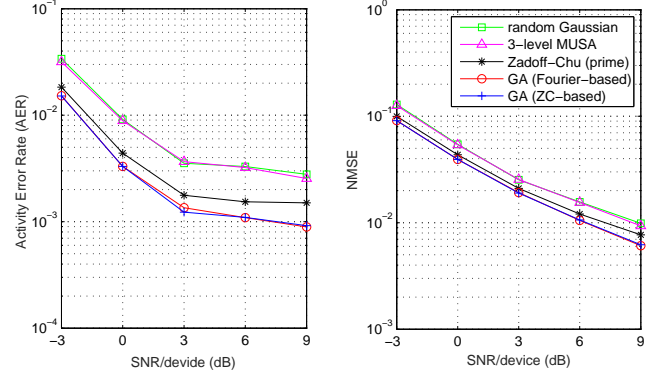


Fig. 7. Performance of CS-based AUD and CE of non-orthogonal sequences over the received SNR per device, where $N = 500$, $M = 80$ ($M_{ZC} = 79$), $J = 16$, and $p_a = 0.1$.

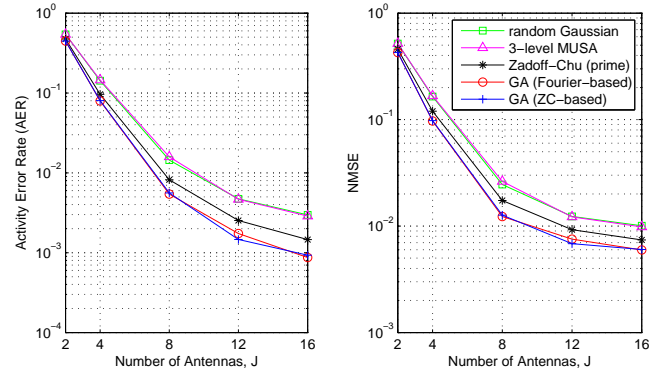


Fig. 8. Performance of CS-based AUD and CE of non-orthogonal sequences over the number of antennas, where $N = 500$, $M = 80$ ($M_{ZC} = 79$), $\text{SNR} = 9$ dB per device, and $p_a = 0.1$.

As a result, the PAPR distributions of the proposed sequences appear to be acceptable for multicarrier transmission.

Fig. 7 shows the performance of CS-based AUD and CE over the received SNR per device. In the figure, the AER and NMSE of Fourier- and ZC-based sequences from our two-stage GA are significantly lower than those of complex-valued random Gaussian and MUSA sequences. The figure also shows that the proposed sequences slightly outperform the ZC sequences of prime length. In addition, Figs. 8 and 9 depict the AER and NMSE over the number of BS antennas and the sequence length, respectively, which also confirm the excellent performance of Fourier- and ZC-based sequences. Taking into account the difference between M and M_{ZC} , we can say that the AUD and CE performance of the proposed sequences are similar to those of the ZC sequences of prime lengths.

C. Discussion

The simulation results of this section demonstrated that the Fourier- and ZC-based sequences designed by our two-stage GA outperform complex-valued random Gaussian and MUSA sequences for CS-based AUD and CE. Also, we observed that the performance of the proposed sequences is similar to that of the ZC sequences of prime lengths.

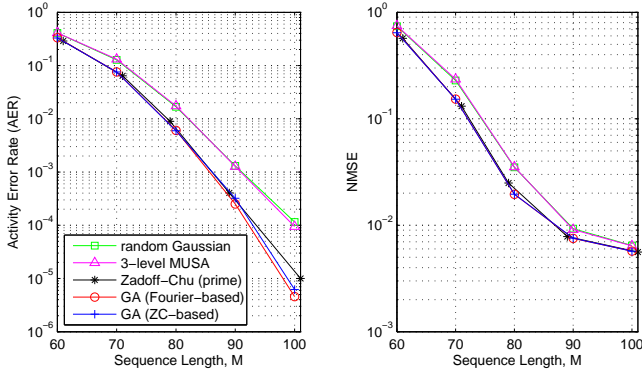


Fig. 9. Performance of CS-based AUD and CE of non-orthogonal sequences over the sequence length, where $N = 500$, $J = 8$, $\text{SNR} = 5$ dB per device, and $p_a = 0.1$. The prime lengths of ZC sequences are $M_{ZC} = 61, 71, 79, 89$, and 101, respectively.

In comparison to the ZC sequences, we would like to point out other potential benefits of the proposed sequences. First, the non-orthogonal sequences from our two-stage GA have no limit to the granularity of sequence length, which suggests that one can obtain the sequences of arbitrary length, according to the availability of resource subcarriers. Meanwhile, the length of the ZC sequences should be odd prime only, which is less flexible for managing resource subcarriers. Being able to take arbitrary sequence lengths, the proposed sequences are expected to facilitate mMTC systems to manage the resources more effectively for grant-free access.

Second, the proposed sequences constitute a partial unitary matrix with a column mask through arbitrary row selection, whereas the ZC sequences of prime length form a deterministic matrix with low coherence. While the coherence-based recovery guarantee of the deterministic matrix is limited by its theoretical bottleneck [17], our partial unitary matrix can present theoretical recovery guarantee with higher sparsity, which ensures reliable CS-based detection theoretically for more active devices in mMTC. In summary, the proposed non-orthogonal sequences can be a good option for uplink grant-free access, supporting any number of subcarriers and providing theoretically guaranteed performance for CS-based AUD and CE. Remarkably, our GA-based design offers a new set of non-orthogonal sequences with many advantages over the ZC sequences of prime length, which are known for the superb performance in practice.

VI. CONCLUSION

This paper has presented a two-stage genetic algorithm (GA) to design new non-orthogonal sequences for uplink grant-free access in mMTC. The first-stage GA is to find a subsampling index set for a partial unitary matrix that can be approximated to an ETF. The second-stage GA then tries to find a masking sequence to be commonly applied to each column of the partial unitary matrix from the first-stage, in order to enhance the PAPR property of the resulting columns. In each stage GA, a new cost function has been elaborately proposed to improve the optimized result. Finally, the masked

columns of the partial unitary matrix are proposed as new non-orthogonal sequences for uplink grant-free access. To the best of our knowledge, this is the first effort to apply the GA technique to non-orthogonal sequence design for achieving low correlation and low PAPR properties simultaneously.

Simulation results demonstrated that the partial Fourier and ZC matrices optimized by our first-stage GA guarantee reliable CS reconstruction over a wide range of compression and sparsity ratios. Also, we observed that the second-stage GA produces the Fourier- and ZC-based sequences that have acceptable PAPR distributions for multicarrier transmission. Finally, we demonstrated that the Fourier- and ZC-based sequences exhibit reliable performance of CS-based AUD and CE in uplink grant-free access, which can be suitable for massive connectivity.

The main benefits of this GA-based design are summarized as follows.

- The non-orthogonal sequences obtained by this GA-based design present theoretical recovery guarantee for CS reconstruction by forming a partial unitary matrix through arbitrary row selection. Simulation results confirmed that the Fourier- and ZC-based sequences from this design show excellent performance of CS-based AUD and CE in uplink grant-free access.
- This GA-based design is able to generate non-orthogonal sequences of arbitrary length, which can be a good choice for sequence lengths for which algebraically designed sequences with low correlation are unknown. In practice, the sequences of arbitrary length can be useful for mMTC systems to manage the resources effectively.
- Based on unitary matrices, this GA-based design can offer unimodular sequences of finite phase with rich structure, which are suitable for cost efficient implementation in mMTC devices.

While this GA-based design successfully presented new non-orthogonal sequences for grant-free massive connectivity, a further study will be necessary to enhance the design method. First, the PAPR of the Fourier- and ZC-based sequences, although improved through evolution, still needs to be reduced further. It will be challenging, but necessary to devise a more elaborate method for further PAPR reduction so that the PAPR distribution of the resulting sequences can be as good as that of the ZC sequences of prime lengths. Second, this GA-based design using the Fourier or ZC matrices increases the number of phases of sequence elements as more sequences are required to support more mMTC devices. To resolve this issue, we have employed the Hadamard matrices for our two-stage GA, but found that the performance of CS-based detection is worse than that of Fourier or ZC matrices. To obtain sequences of small phase, we may need to study further with another unitary matrix of high dimension but with each element of smaller phase. Third, the proposed non-orthogonal sequences are for a single-cell massive connectivity, but a further study will be necessary for this GA-based design to provide multiple sets of non-orthogonal sequences for multi-cell environments. Finally, our two-stage GA can be considered as a component of DL-based sequence design, which is our ongoing research work.

REFERENCES

- [1] T. Taleb and A. Kunz, "Machine type communications in 3GPP networks: Potential, challenges, and solutions," *IEEE Commun. Mag.*, vol. 50, no. 3, pp. 178-184, Mar. 2012.
- [2] C. Bockelmann *et al.*, "Massive machine-type communications in 5G: Physical and MAC-layer solutions," *IEEE Commun. Mag.*, vol. 54, no. 9, pp. 59-65, Sep. 2016.
- [3] 3GPP TS 22.368, V13.1.0, *Service Requirements for Machine-type Communications (MTC)*, Release 13, 2015.
- [4] L. Dai, B. Wang, Y. Yuan, S. Han, C.-L. I, and Z. Wang, "Non-orthogonal multiple access for 5G: Solutions, challenges, opportunities, and future research trends," *IEEE Commun. Mag.*, vol. 53, no. 9, pp. 74-81, Sep. 2015.
- [5] L. Dai, B. Wang, Z. Ding, Z. Wang, S. Chen, and L. Hanzo, "A survey of non-orthogonal multiple access for 5G," *IEEE Commun. Surveys & Tut.*, vol. 20, no. 3, pp. 2294-2323, 2018.
- [6] H. Nikopour and H. Baligh, "Sparse code multiple access," *Proc. IEEE 24th Int. Symp. Pers. Indoor Mobile Radio Commun. (IEEE PIMRC)*, London, U.K., Sep. 2013, pp. 332-336.
- [7] S. Zhang *et al.*, "Sparse code multiple access: An energy efficient uplink approach for 5G wireless systems," *Proc. IEEE Glob. Commun. Conf. (IEEE GLOBECOM)*, Austin, TX, USA, Dec. 2014, pp. 4782-4787.
- [8] F. Wei and W. Chen, "A low complexity SCMA decoder based on list sphere decoding," *Proc. IEEE Glob. Commun. Conf. (IEEE GLOBECOM)*, Washington, DC, USA, Dec. 2016, pp. 1-6.
- [9] Z. Yuan, G. Yu, W. Li, Y. Yuan, X. Wang, and J. Xu, "Multi-user shared access for Internet of Things," *IEEE 83rd Veh. Technol. Conf. (VTC Spring)*, pp. 1-5, China, May 15-18, 2016.
- [10] S. Kang, X. Dai, and B. Ren, "Pattern division multiple access for 5G," *Telecommun. Netw. Technol.*, vol. 5, no. 5, pp. 43-47, May 2015.
- [11] M. V. Jamali and H. Mahdavi, "A Low-complexity recursive approach toward code-domain NOMA for massive communications," *Proc. IEEE Glob. Commun. Conf. (IEEE GLOBECOM)*, Abu Dhabi, United Arab Emirates, 2018, pp. 1-6.
- [12] I. Goodfellow, Y. Bengio, and A. Courville, *Deep Learning*, Cambridge, MA, USA: MIT Press, 2016.
- [13] N. Ye, X. Li, H. Yu, L. Zhao, W. Liu, and X. Hou, "DeepNOMA: A unified framework for NOMA using deep multi-task learning," *IEEE Trans. Wireless Commun.*, vol. 19, no. 5, pp. 2208-2225, Apr. 2020.
- [14] W. Kim, Y. Ahn, and B. Shim, "Deep neural network-based active user detection for grant-free NOMA systems," *IEEE Trans. Commun.*, vol. 68, no. 4, pp. 2143-2155, Apr. 2020.
- [15] T. Sivalingam, S. Ali, N. H. Mahmood, N. Rajatheva, and M. Latva-Aho, "Deep neural network-based blind multiple user detection for grant-free multi-user shared access," *arXiv:2106.11204v1 [cs.IT]*, Jun. 2021.
- [16] A. C. Cirik, N. M. Balasubramanya, L. Lampe, G. Vos, and S. Bennett, "Toward the standardization of grant-free operation and the associated NOMA strategies in 3GPP," *IEEE Communications Standards Magazine*, vol. 3, no. 4, pp. 60-66, Dec. 2019.
- [17] Y. C. Eldar and G. Kutyniok, *Compressed Sensing: Theory and Applications*, Cambridge, UK: Cambridge Univ. Press, 2012.
- [18] A. T. Abebe and C. G. Kang, "Iterative order recursive least square estimation for exploiting frame-wise sparsity in compressive sensing-based MTC," *IEEE Commun. Lett.*, vol. 20, no. 5, pp. 1018-1021, May 2016.
- [19] C. Wei, H. Liu, Z. Zhang, J. Dang, and L. Wu, "Approximate message passing-based joint user activity and data detection for NOMA," *IEEE Commun. Lett.*, vol. 21, no. 3, pp. 640-643, Mar. 2017.
- [20] A. Cirik, N. M. Balasubramanya, and L. Lampe, "Multi-user detection using ADMM-based compressive sensing for uplink grant-free NOMA," *IEEE Wireless Commun. Lett.*, vol. 7, no. 1, pp. 46-49, Feb. 2018.
- [21] L. Liu and W. Yu, "Massive connectivity with massive MIMO - part I: Device activity detection and channel estimation," *IEEE Trans. Signal Process.*, vol. 66, no. 11, pp. 2933-2946, June 2018.
- [22] L. Liu, E. G. Larsson, W. Yu, P. Popovski, C. Stefanovic and E. de Carvalho, "Sparse signal processing for grant-free massive connectivity: A future paradigm for random access protocols in the internet of things," *IEEE Signal Process. Mag.*, vol. 35, no. 5, pp. 88-99, Sept. 2018.
- [23] J. Ahn, B. Shim, and K. B. Lee, "EP-based joint active user detection and channel estimation for massive machine-type communications," *IEEE Trans. Commun.*, vol. 67, no. 7, pp. 5178-5189, July 2019.
- [24] X. Shao, X. Chen and R. Jia, "A dimension reduction-based joint activity detection and channel estimation algorithm for massive access," *IEEE Trans. Signal Process.*, vol. 68, pp. 420-435, 2020.
- [25] S. Jiang, X. Yuan, X. Wang, C. Xu, and W. Yu, "Joint user identification, channel estimation, and signal detection for grant-free NOMA," *IEEE Trans. Wirel. Commun.*, vol. 19, no. 10, pp. 6960-6976, Oct. 2020.
- [26] B. Wang, L. Dai, T. Mir, and Z. Wang, "Joint user activity and data detection based on structured compressive sensing for NOMA," *IEEE Commun. Lett.*, vol. 20, no. 7, pp. 1473-1476, July 2016.
- [27] B. Wang, L. Dai, Y. Zhang, T. Mir and J. Li, "Dynamic compressive sensing-based multi-user detection for uplink grant-free NOMA," *IEEE Commun. Lett.*, vol. 20, no. 11, pp. 2320-2323, Nov. 2016.
- [28] Y. Du *et al.*, "Efficient multi-user detection for uplink grant-free NOMA: Prior-information aided adaptive compressive sensing perspective," *IEEE J. Sel. Areas Commun.*, vol. 35, no. 12, pp. 2812-2828, Dec. 2017.
- [29] Y. Du, B. Dong, W. Zhu, P. Gao, Z. Chen, X. Wang, and J. Fang, "Joint channel estimation and multiuser detection for uplink grant-free NOMA," *IEEE Wireless Commun. Lett.*, vol. 7, no. 4, pp. 682-685, Aug. 2018.
- [30] Y. Du, C. Cheng, B. Dong, Z. Chen, X. Wang, J. Fang, and S. Li, "Block-sparsity-based multiuser detection for uplink grant-free NOMA," *IEEE Trans. Wireless Commun.*, vol. 17, no. 12, pp. 7894-7909, Dec. 2018.
- [31] N. Y. Yu, "Multiuser activity and data detection via sparsity-blind greedy recovery for uplink grant-free NOMA," *IEEE Commun. Lett.*, vol. 23, no. 11, pp. 2082-2085, Nov. 2019.
- [32] M. Ke, Z. Gao, Y. Wu, X. Gao, and R. Schober, "Compressive sensing-based adaptive active user detection and channel estimation: Massive access meets massive MIMO," *IEEE Trans. Signal. Process.*, vol. 68, pp. 764-779, 2020.
- [33] S. Litsyn, *Peak Power Control in Multicarrier Communications*, Cambridge University Press, 2007.
- [34] G. Wunder, R. F. H. Fischer, H. Boche, S. Litsyn and J.-S. No, "The PAPR problem in OFDM transmission: New directions for a long-lasting problem" *IEEE Signal Process. Mag.*, vol. 30, no. 6, pp. 130-144, Nov. 2013.
- [35] A. S. Rajasekaran, M. Vameghestahbanati, M. Farsi, H. Yanikomegoglu, and H. Saedi, "Resource allocation-based PAPR analysis in uplink SCMA-OFDM systems," *IEEE Access*, vol. 7, pp. 162803-162817, 2019.
- [36] Z. Mheich, L. Wen, P. Xiao, and A. Maaref, "Design of SCMA codebooks based on golden angle modulation," *IEEE Trans. Veh. Technol.*, vol. 68, no. 2, pp. 1501-1509, Feb. 2019.
- [37] K. Yang, Y.-K. Kim, and P. V. Kumar, "Quasi-orthogonal sequences for code-division multiple-access system," *IEEE Trans. Inf. Theory*, vol. 46, no. 3, pp. 982-993, May 2000.
- [38] M. J. E. Golay, "Complementary series," *IRE Trans. Inf. Theory*, vol. IT-7, pp. 82-87, 1961.
- [39] J. A. Davis and J. Jedwab, "Peak-to-mean power control in OFDM, Golay complementary sequences, and Reed-Muller codes," *IEEE Trans. Inf. Theory*, vol. 45, no. 7, pp. 2397-2417, Nov. 1999.
- [40] K. G. Paterson, "Generalized Reed-Muller codes and power control in OFDM modulation," *IEEE Trans. Inf. Theory*, vol. 46, no. 1, pp. 104-120, Jan. 2000.
- [41] Z. Liu, P. Xiao, and S. Hu, "Low-PAPR preamble design for FBMC systems," *IEEE Trans. Veh. Technol.*, vol. 68, no. 8, pp. 7869-7876, Aug. 2019.
- [42] N. Y. Yu, "Binary Golay spreading sequences and Reed-Muller codes for uplink grant-free NOMA," *IEEE Trans. Commun.*, vol. 69, no. 1, pp. 276-290, Jan. 2021.
- [43] N. Y. Yu, "Non-orthogonal Golay-based spreading sequences for uplink grant-free access," *IEEE Commun. Lett.*, vol. 24, no. 10, pp. 2104-2108, Oct. 2020.
- [44] Z. Liu, Y. L. Guan, and U. Parampalli, "New complete complementary codes for peak-to-mean power control in multicarrier CDMA," *IEEE Trans. Commun.*, vol. 62, no. 3, pp. 1105-1113, Mar. 2014.
- [45] Y. Li and C. Xu, "ZCZ aperiodic complementary sequence sets with low column sequence PMEPR," *IEEE Commun. Lett.*, vol. 19, no. 8, pp. 1303-1306, Aug. 2015.
- [46] T. Jiang, C. Ni and Y. Xu, "Novel 16-QAM and 64-QAM near-complementary sequences with low PMEPR in OFDM systems," *IEEE Trans. Commun.*, vol. 64, no. 10, pp. 4320-4330, Oct. 2016.
- [47] C. Chen, "Complementary sets of non-power-of-two length for peak-to-average power ratio reduction in OFDM," *IEEE Trans. Inf. Theory*, vol. 62, no. 12, pp. 7538-7545, Dec. 2016.
- [48] S. Wu and C. Chen, "Optimal Z-complementary sequence sets with good peak-to-average power-ratio property," *IEEE Signal Process. Lett.*, vol. 25, no. 10, pp. 1500-1504, Oct. 2018.
- [49] C. Chu, "Polyphase codes with good periodic correlation properties," *IEEE Trans. Inf. Theory*, vol. 18, no. 4, pp. 531-532, Jul. 1972.
- [50] 3GPP TS 36.211 V13.1.0, *Physical Channel and Modulation*, Mar. 2016.

- [51] M. Elad, "Optimized projections for compressed sensing," *IEEE Trans. Sig. Proc.*, vol. 55, no. 12, pp. 5695-5702, Dec. 2007.
- [52] J. Xu, Y. Pi, and Z. Cao, "Optimized projection matrix for compressive sensing," *EURASIP J. Adv. Signal Process.*, vol. 2010, 2010.
- [53] V. Abolghasemi, S. Ferdowsi, and S. Sanei, "A gradient-based alternating minimization approach for optimization of the measurement matrix in compressive sensing," *Signal Process.*, vol. 92, pp. 999-1009, 2012.
- [54] G. Li, Z. Zhu, D. Yang, L. Chang, and H. Bai, "On projection matrix optimization for compressive sensing systems," *IEEE Trans. Sig. Proc.*, vol. 61, no. 11, pp. 2887-2898, Jun. 2013.
- [55] Q. Xu, Z. Sheng, Y. Fang, and L. Zhang, "Measurement matrix optimization for compressed sensing system with constructed dictionary via Takenaka-Malmquist functions," *Sensors* 21, no. 4: 1229, 2021.
- [56] J. Kovacevic and A. Chebira, *An Introduction to Frames*, Foundations and Trends in Signal Processing, now Publishers Inc., 2008.
- [57] W. Chen, M. R. D. Rodrigues, and I. J. Wassell, "On the use of unit-norm tight frames to improve the average MSE performance in compressive sensing applications," *IEEE Sig. Process. Lett.*, vol. 19, no. 1, pp. 8-11, Jan. 2012.
- [58] J. M. Duarte-Carvajalino and G. Sapiro, "Learning to sense sparse signals: simultaneous sensing matrix and sparsifying dictionary optimization," *IEEE Trans. Imag. Process.*, vol. 18, no. 7, pp. 1935-1408, 2009.
- [59] C. Lu, H. Li, and Z. Lin, "Optimized projections for compressed sensing via direct mutual coherence minimization," *Signal Process.*, vol. 151, pp. 45-55, 2018.
- [60] C. Chun, J. Kang and I. Kim, "Deep learning-based joint pilot design and channel estimation for multiuser MIMO channels," *IEEE Commun. Lett.*, vol. 23, no. 11, pp. 1999-2003, Nov. 2019.
- [61] N. Kim, D. Kim, B. Shim and K. B. Lee, "Deep learning-based spreading sequence design and active user detection for massive machine-type communications," *IEEE Wirel. Commun. Lett.*, Early Access, June 2021.
- [62] J. H. Holland, *Adaptation in Natural and Artificial Systems: An Introductory Analysis With Applications to Biology, Control and Artificial Intelligence*, Cambridge, MA, USA: MIT Press, 1992.
- [63] Y.-J. Chen, Q. Zhang, Y. Luo, and Y.-A. Chen, "Measurement matrix optimization for ISAR sparse imaging based on genetic algorithm," *IEEE Geoscience Remote Sens. Lett.*, vol. 13, no. 12, pp. 1875-1879, Dec. 2016.
- [64] Y. Nie, X. Yu, and Z. Yang, "Deterministic pilot pattern allocation optimization for sparse channel estimation based on CS theory in OFDM system," *EURASIP J. Wirel. Commun. Netw.*, 2019:7, 2019.
- [65] M. A. Mazaideh and J. Levendovszky, "A multi-hop routing algorithm for WSNs based on compressive sensing and multiple objective genetic algorithm," *Journ. of Commun. Netw.*, vol. 23, no. 2, pp. 138-147, Apr. 2021.
- [66] L. R. Welch, "Lower bounds on the maximum cross correlation of signals," *IEEE Trans. Inf. Theory*, vol. IT-20, no. 3, pp. 397-399, May 1974.
- [67] M. Duarte and Y. C. Eldar, "Structured compressed sensing: From theory to applications," *IEEE Trans. Signal Process.*, vol. 59, no. 9, pp. 4053-4085, Sep. 2011.
- [68] M. Rudelson and R. Vershynin, "On sparse reconstruction from Fourier and Gaussian measurements," *Comm. Pure Appl. Math.*, vol. 61, no. 8, pp. 1025-1045, Aug. 2008.
- [69] A. A. Freitas, "A survey of evolutionary algorithms for data mining and knowledge discovery," *Advances in Evolution. Comput.*, Springer-Verlag, pp. 819-845, 2002.
- [70] L. Yang, D. H. Widyantoro, T. Ioerger, and J. Yen, "An entropy-based adaptive genetic algorithm for learning classification rules," *Proc. 2001 Congress Evolution. Comput.*, pp. 790-796, 2001.
- [71] P. Vivekanandan, M. Rajalakshmi, and R. Nedunchezian, "An intelligent genetic algorithm for mining classification rules in large data sets," *Computing and Informatics*, vol. 32, pp. 1-22, 2013.
- [72] L. Hebbes, R. R. Malyan, and A. P. Lenaghan, "Genetic algorithms for turbo codes," *Proc. Int Conf. Comput. Tool.*, vol. 1, pp. 478-481, Nov. 2005.
- [73] H. Maini, K. Mehrotra, C. Mohan, and S. Ranka, "Genetic algorithms for soft-decision decoding of linear block codes," *Evol. Comput.*, vol. 2, no. 2, pp. 145-164, Jun. 1994.
- [74] A. Scandura, A. D. Pra, L. Arnone, L. I. Passoni, and J. C. Moreira, "A genetic-algorithm based decoder for low density parity check codes," *Latin Amer. Appl. Res.*, vol. 36, no. 3, pp. 169-172, Jul. 2006.
- [75] A. Elkelesh, M. Ebada, S. Crammerer, and S. ten Brink, "Decoder-tailored polar code design using the genetic algorithm," *IEEE Trans. Commun.*, vol. 67, no. 7, pp. 4521-4534, Jul. 2019.
- [76] H. H. Dam, H.-J. Zepernick, and H. Luders, "On the design of complex-valued spreading sequences using a genetic algorithm," *IEEE ISSTA*, pp. 704-707, Sydney, Australia, Aug., 2004.
- [77] B. Natarajan, S. Das, and D. Stevens, "An evolutionary approach to designing complex spreading codes for DS-CDMA," *IEEE Trans. Wirel. Commun.*, vol. 4, no. 5, pp. 2051-2056, Sep. 2005.
- [78] M. H. Conde and O. Loffeld, "A genetic algorithm for compressive sensing sparse recovery," *IEEE Int. Symp. Signal Process. Inf. Technol.*, pp. 106-111, 2017.
- [79] H. You and J. Zhu, "A genetic approach to fusion of algorithms for compressive sensing," *Int. Symp. Neural Netw., Advances in Neural Networks-ISNN2017*, pp. 371-379, Springer, 2017.
- [80] M. E. Erkoç and N. Karaboga, "Evolutionary algorithms for sparse signal reconstruction," *Signal, Image and Video Processing*, vol. 13, pp. 1293-1301, Springer-Verlag London Ltd., 2019.
- [81] J. A. Tropp, A. C. Gilbert, and M. J. Strauss, "Algorithms for simultaneous sparse approximation. Part I: Greedy pursuit," *Signal Process.*, vol. 86, pp. 572-588, Apr. 2006.
- [82] D. V. Sarwate, "Bounds on crosscorrelation and autocorrelation of sequences," *IEEE Trans. Inf. Theory*, vol. IT-25, no. 6, pp. 720-724, Nov. 1979.